Critical behavior of two molecular magnets probed by complementary experiments

M. Czapla,* R. Pełka, P. M. Zieliński, A. Budziak, M. Bałanda, M. Makarewicz, A. Pacyna, and T. Wasiutyński
H. Niewodniczański Institute of Nuclear Physics, Polish Academy of Sciences, Radzikowskiego 152, 31-342 Kraków, Poland

Yuji Miyazaki, Yasuhiro Nakazawa, Akira Inaba, and Michio Sorai
Research Center for Structural Thermodynamics, Graduate School of Science, Osaka University, Toyonaka, Osaka, Japan

F. L. Pratt
ISIS Facility, Rutherford Appleton Laboratory, Chilton, Oxfordshire OX11 0QX, United Kingdom

R. Podgajny, T. Korzeniak, and B. Sieklucka
Department of Chemistry, Jagiellonian University, Ingardena 3, Kraków, Poland

(Received 14 July 2010; revised manuscript received 6 September 2010; published 29 September 2010)

The fast developing field of molecule-based magnets involving organic and coordination chemistry provides the physicist with a multitude of novel compounds of unprecedented structure. The magnetic structure of $Cu_4(tetren)[W(CN)_8]_4$ (**1**) was shown to consist of weakly coupled double layers. By contrast, in the structurally similar compound $Cu_{2+x}Cu_4[W(CN)_8]_4$ (**2**) the free spaces between the double layers are filled with paramagnetic copper(II) ions leading to a unique magnetic network. Both compounds exhibit the transition to a magnetically ordered phase at $T_c \approx 33$ K and $T_c \approx 40$ K, respectively. The critical behavior of **1** and **2** is investigated using complementary methods: ac magnetometry, relaxation calorimetry, and muon spin-rotation spectroscopy. Apart from α, β, and γ, critical exponents κ and κ' describing the combined scaling of excess entropy and order parameter are determined for both compounds. This type of scaling is verified for **1**, the system revealing the signatures of the Berezinskii-Kosterlitz-Thouless transition. For **2** their values imply that the system is close to the universality class of the three-dimensional Heisenberg model. The relatively small value of exponent $\gamma=1.05$ for **2** indicates the presence of noncollinearity in the spin arrangement. Exponents κ and κ' for **2** are also found consistent with noncollinear models. The shift of the heat-capacity anomaly toward higher temperatures with increasing applied field indicates the presence of ferromagnetic interactions in **2**.

DOI: 10.1103/PhysRevB.82.094446 PACS number(s): 75.50.Xx, 75.40.Cx, 76.75.+i

I. INTRODUCTION

Molecular magnetism has been ceaselessly of major interest for the last decades. Extensive studies of molecule-based magnets revealed a number of striking features such as room-temperature molecular magnets,[1] single-molecule[2] or single-chain magnets,[3,4] photoinduced magnets,[5–7] magnetic spongelike behavior,[8,9] to name but a few. One of the promising aspects of these materials is the fact that their properties can be modulated by flexible organic synthesis methods. Interestingly, by appropriately tuning the synthesis path one can affect the dimensionality of the ensuing magnetic system. Among a large number of ligands the cyanido anions play a crucial role in the engineering of such materials and lead to the variety of structures and functionalities.[10–13]

Molecular magnets belong mostly to the class of compounds involving well-localized magnetic moments. For this reason they provide a unique experimental ground for testing the existing theoretical spin models. The signatures of the nature and symmetry of magnetic interactions are encrypted in the values of the corresponding critical exponents. This makes the studies of critical behavior an appealing field complementary to other methods aimed at full understanding of magnetic couplings in a system. Besides, molecular compounds represent sometimes examples of unique magnetic structures, unprecedented in conventional materials. The physical characterization of those is an important contribution to the understanding of the diversity of magnetic systems. The present work deals with such an example of a very specific magnetic structure.

In this work we focus on the critical behavior in two cyanido-bridged molecular magnets displaying different dimensionalities of the magnetic network. Recently, we have shown that compound $\{(tetrenH_5)_{0.8}Cu^{II}_4[W^V(CN)_8]_4 \cdot 7H_2O\}_n$ (tetren=tetraethylenepentamine), which will be referred to as compound **1**, revealed the signatures of the Berezinskii-Kosterlitz-Thouless (BKT) transition at $T_c \approx 33$ K with critical exponents close to those of the two-dimensional (2D) XY model.[14,15] Crystal structure of **1** was solved by the single-crystal x-ray diffraction[16] and is depicted in Fig. 1. The compound crystallizes in the orthorhombic system (space group $Cmc2_1$) with unit-cell parameters $a=7.3792(6)$ Å, $b=32.096(2)$ Å, and $c=7.0160(6)$ Å. It consists of anionic double layers formed by copper and tungsten ions distributed over the layers in an alternating fashion and linked through the cyanido bridges. Within the double-layer each Cu(II) ion is surrounded by five NC bridges connecting it to the neighboring W(V) ions whereas the coordination sphere of each W(V) ion comprises eight cyanido ligands. Five of them mediate the linkage to the neighboring Cu(II) ions, and the three remaining ones stand out of the double layers and are presumably involved in the network of hydrogen bonds. The space between the double layers is filled with water molecules and the fully protonated $tetrenH_5$

 ©2010 The American Physical Society

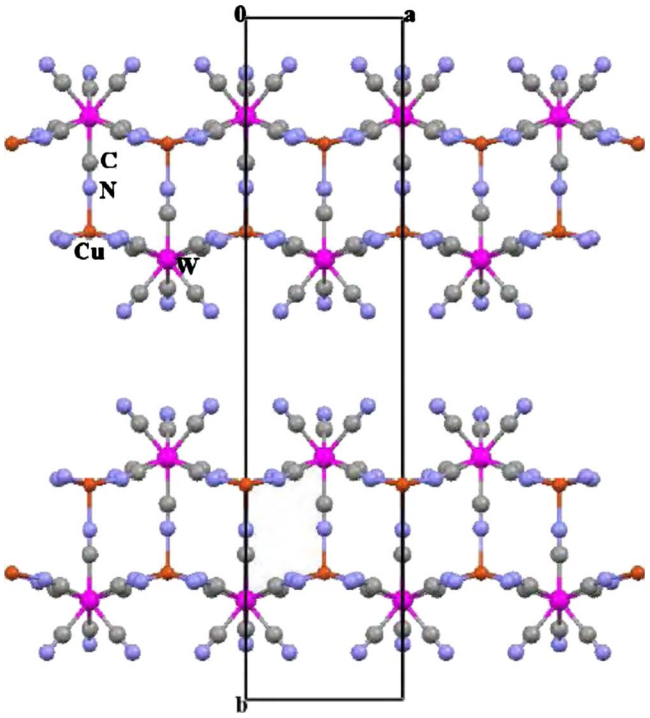

FIG. 1. (Color online) Projection of the crystal structure of **1** onto the *ab* crystallographic plane. Alternating arrangement of Cu(II) and W(V) ions forms anionic double layers. The space between them is filled with tetrenH_5 countercations and water molecules (not shown for clarity).

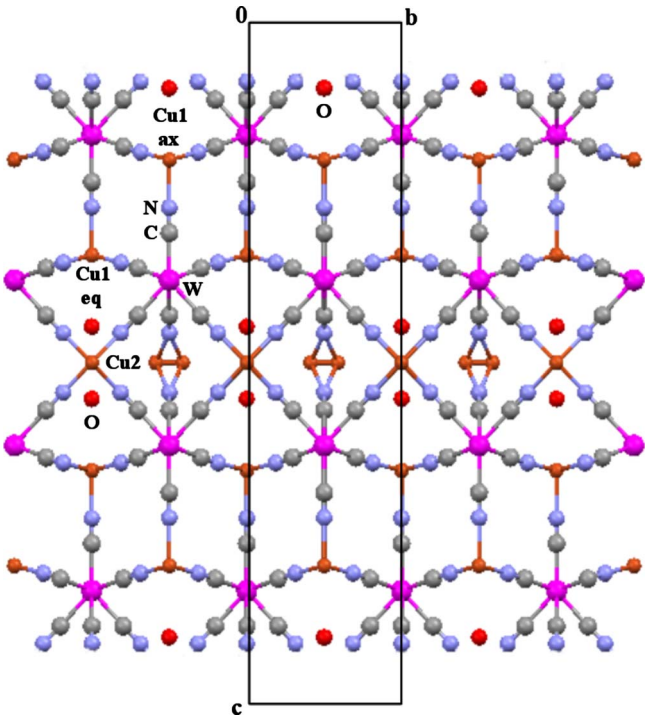

FIG. 2. (Color online) Projection of the crystal structure of **2** onto the *bc* crystallographic plane. The system of Cu(II)-W(V) double layers is similar as in **1**. The space between them is filled with additional paramagnetic Cu(II) ions and water molecules, of which only oxygen atoms are shown.

molecules to maintain the charge balance. Magnetic interaction between the double layers, related to the rather large interbilayer distance of about 10 Å, stems from two independent sources. On the one hand, we can expect the exchange coupling through the system of hydrogen bonds and, on the other hand, the through space dipole-dipole interactions become comparable to the exchange interaction due to the rather large interbilayer distance.

Compound **2** was produced by withdrawing the tetren molecule from the synthesis path of **1** with the view to enhance the magnetic coupling between the double layers. In consequence, additional Cu(II) ions were located in the interlayer spaces and the magnetic transition temperature was raised up to 40 K. The compound crystallizes in the tetragonal system with space group $I4/mmm$ and unit-cell parameters: $a=b=7.22858(9)$ Å, $c=28.282(5)$ Å.[17] Figure 2 shows the projection of the crystal structure of **2** onto the *bc* crystallographic plane. Its chemical formula $Cu^{II}_{2+x}\{Cu^{II}_4[W^V(CN)_8]_{4-2x}[W^{IV}(CN)_8]_{2x}\}\cdot 4H_2O$ indicates that there is a weakly nonstoichiometric amount of Cu(II) ions placed between the double layers. To satisfy the charge balance the nonstoichiometric diamagnetic W(IV) ions appear in the double-layer skeleton. The value of x indicated by the Rietveld refinement of the x-ray diffraction pattern is 0.97. The presence of the diamagnetic species affects the distribution of the exchange coupling in the crystal. However, it does not preclude the formation of the three-dimensional (3D) extended network of coupled spins. Another important structural feature of **2** is the distribution of the interdouble-layer Cu(II) ions. Structural data indicate that the additional Cu(II) ions can take four equivalent positions lying above the centers of the squares of the double-layer grid. The formula of **2** implies that the occupation probability of each position is approximately 3/8. This imbalance between the number of possible positions and the number of the available Cu(II) reduces exchange coupling between the double layers. The presence of nonstoichiometric amounts of diamagnetic W(IV) ions and paramagnetic Cu(II) ions between the double layers together with the partial occupation of available sites by the latter may lead to the disorder of the magnetic network.

In the present contribution we focus on the critical behavior of these two structurally related compounds. To determine the corresponding critical exponents complementary experimental methods have been used ranging from the magnetic ac susceptibility measurements, through the calorimetric measurements up to the muon spin-rotation (μSR) technique. Apart from the standard critical exponents α, β, and γ this wide spectrum of experiments enabled to estimate the exponents κ and κ' appearing in the combined scaling of excess entropy and order parameter.

The paper is organized as follows. Section II lists the details of experimental techniques used. In Sec. III the results of the neutron powder diffraction for **2** are presented and discussed. Section IV deals with the critical behavior as revealed by the ac magnetic susceptibility measurement. In Sec. V heat-capacity measurements of **2** are reported and interpreted. In Sec. VI the measurements by the μSR technique are presented giving insight into the thermal dependence of order parameter. That information together with the

output of calorimetric measurements for both compounds are used to reveal the combined scaling of the excess entropy and order parameter, which is described in Sec. VII. Section VIII includes final remarks and conclusions.

II. EXPERIMENTAL

The neutron powder-diffraction measurements were performed on D20 instrument at ILL facility in Grenoble using neutron wavelength $\lambda = 1.88$ Å. First, the sample was cooled down to 2 K and next the diffraction patterns were detected at subsequent temperatures 2, 35, and 45 K. The D20 instrument was chosen as it provides high beam intensity crucial for systems involving low-spin values. Magnetic measurements of **2** were carried out with the Lake Shore 7225 instrument in the temperature range of 4.2–250 K, in zero dc field, and with $H_{ac}=5$ Oe and $f=125$ Hz. The heat-capacity measurements were performed with the Physical Property Measurement System (PPMS) Quantum Design instrument by the relaxation calorimetry technique on a powder sample in the temperature range of 2–300 K and for several values of external magnetic field in the range of 0–90 kOe. The μSR experiment was performed at the ISIS pulsed muon facility using the μSR instrument. The polycrystalline powder sample wrapped in the silver foil was mounted in the sample holder and placed in the cryostat employing a helium bath to give temperatures down to 1.8 K. Prior to the experiment the instrument was calibrated at 50 K and transverse field of 20 G. Next, the sample was cooled down to 2 K in zero external field, and the measurement was repeated for an array of temperatures reaching a few kelvin above the transition point. The output of the μSR experiment was analyzed with WIMDA software.[18]

III. NEUTRON POWDER DIFFRACTION

The crystal structure of **2** detected at room temperature was already reported in Ref. 17. Additional measurements were performed to get insight into temperature behavior of the sample and also into the magnetic structure below the transition at $T_c \approx 40$ K. To achieve this goal neutron powder-diffraction technique was applied. The top panel of Fig. 3 shows the corresponding patterns for 2, 35, and 45 K. It can be seen that in spite of the large background due to incoherent scattering, the Bragg peaks are well defined. The bottom panel of Fig. 3 depicts the difference between the signals detected at 2 K (below the transition point) and 45 K (above the transition point). Strikingly, the subtraction of the patterns reveals no significant difference, i.e., no additional Bragg peaks corresponding to low-temperature magnetic structure are present as well as no substantial increase in the intensity of the existing peaks is observed. This may be due to the fact that the compound contains centers Cu(II) and W(V) carrying spin one-half, and the corresponding Bragg magnetic peaks are expected to be of low intensity and may be hidden by the relatively stronger ones coming from the crystal structure. Additionally, the possible presence of diamagnetic W(IV) ions implies the formation of disjoint clusters of coupled spins. Secondly, the partial occupancy of the interdouble-layer sites of the Cu(II) ions may lead to irregularities in spin distribution. Both facts are expected to reduce the contribution to the intensity of scattered neutrons.

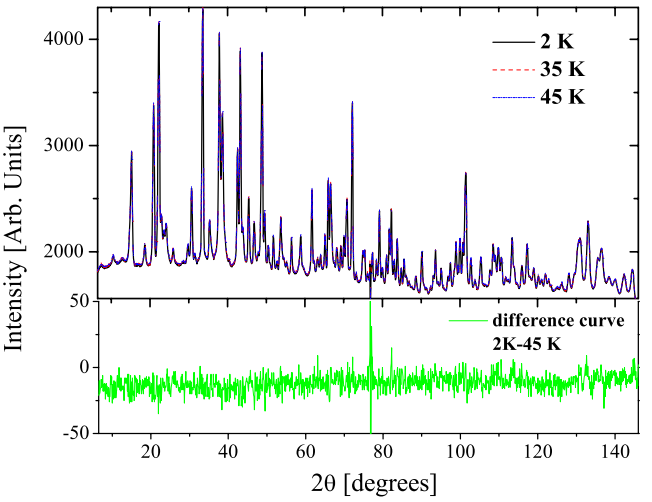

FIG. 3. (Color online) Top panel: powder-diffraction patterns for **2** recorded at 2, 35, and 45 K. Above considerable background due to incoherent scattering well-defined Bragg peaks are present. Bottom panel: comparison of the diffraction patterns detected at 45 K (above magnetic transition) and 2 K (below magnetic transition). No additional Bragg peaks and no intensity enhancement of the existing peaks are observed.

IV. ac SUSCEPTIBILITY

Figure 4 shows real component χ' of the ac susceptibility signal for **1** and **2**. For both compounds very sharp peaks at $T_c=33.04$ K (**1**) and $T_c=39.9$ K (**2**) are observed revealing the transition to an ordered phase. In comparison to **1** the ordering temperature of **2** is shifted to higher values. This corresponds well with the fact that compound **2** contains additional Cu(II) ions located between the structural double

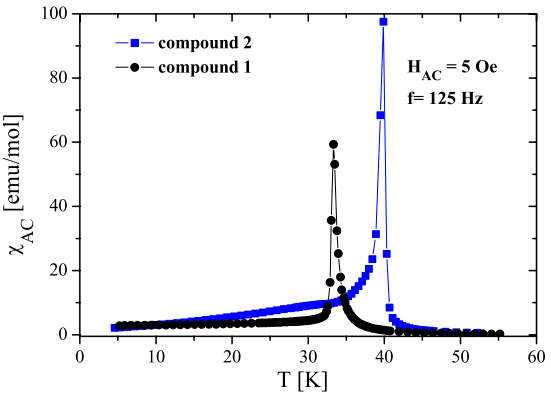

FIG. 4. (Color online) Real part of ac magnetic susceptibility for **1** and **2**. For both compounds sharp anomalies at $T_c=33.04$ K and $T_c=39.9$ K, respectively, mark the transition to the magnetically ordered phase. Higher transition temperature of **2** is attributed to the presence of additional Cu(II) ions exchange coupled with the spin centers constituting the double-layer sheets.

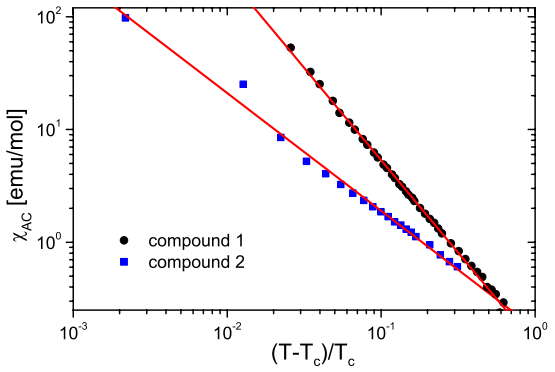

FIG. 5. (Color online) Classical scaling analysis of the ac susceptibility signals for **1** and **2**. The value of the gamma exponent of the quasi-2D spin network (compound **1**) is enhanced as compared to that of compound **2** displaying the 3D connectivity of spin centers.

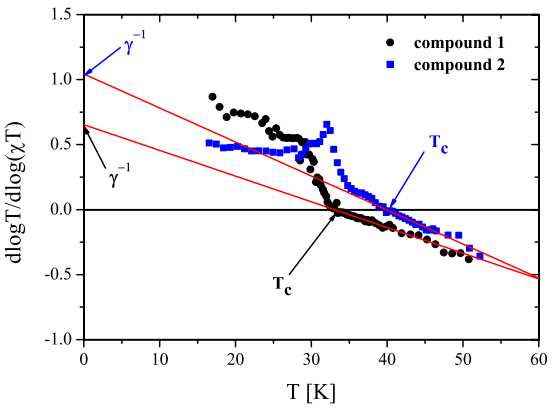

FIG. 6. (Color online) Scaling analysis of the ac susceptibility signals for **1** and **2**. The intercepts of the best-fit curves (solid lines) with both axes yield T_c and $1/\gamma$. The value of the gamma exponent of the quasi-2D spin network (compound **1**) is enhanced as compared to that of compound **2** displaying the 3D connectivity of spin centers.

layers providing with the cyanido bridges the interbilayer magnetic linkage, the feature absent in **1**. There is an apparent difference in the high-temperature slope of the ac signal between compounds **1** and **2**, which suggests distinct critical behavior and a possible change in the dimensionality of the corresponding magnetic network. The more gentle high-temperature slope of the susceptibility curve of compound **1** may most probably be attributed to the 2D character of spin fluctuations. No frequency dependence of χ' of **1** and **2** was detected excluding spin-glass behavior. The single-crystal study of **1** (Ref. 14) revealed weak metamagnetism with spin-flop field on the order of 50 Oe. Unlike for **1**, on the low-temperature wing of the ac signal of **2** an elevated shoulder can be seen. Its position coincides roughly with the position of the χ' peak of **1**. This feature is probably related to the presence of the strong easy-plane anisotropy detected for **1** (Ref. 14) and may signal a crossover to a new state of magnetic order with spins pointing in the easy direction. To get insight into the critical behavior for both compounds, two types of static scaling analysis of χ were performed. The first one is based on the classical scaling relation

$$\chi = c\left(\frac{T - T_c}{T_c}\right)^{-\gamma} \tag{1}$$

while the other draws on the modified scaling law put forward by Carré and Souletie (CS),[19,20] where the critical behavior is described by the formula

$$\chi T = c\left(1 - \frac{T_c}{T}\right)^{-\gamma}. \tag{2}$$

It was demonstrated[20] that this law is applicable in an extended temperature range as compared to the standard scaling law given by Eq. (1), thus allowing for a more certain determination of the critical exponent. It is useful to perform a nonlinear transformation of Eq. (2) and get

$$\left(\frac{\partial \log(\chi T)}{\partial \log T}\right)^{-1} = -\gamma^{-1}\frac{T - T_c}{T_c}, \tag{3}$$

which is expected to put the data points on a straight line. Additionally, the intersection point of this straight line with the temperature axis gives the transition temperature whereas at the same time the intersection point with the vertical axis gives the inverse of the gamma exponent. The results shown in Figs. 5 and 6 indicate a significant difference between the two samples. In Table I the results of both approaches are listed. It can be seen that both types of scaling give more consistent γ values for the quasi-2D compound **1** than for the 3D spin network of compound **2**. The discrepancy for the latter may be due to the fact that the modified scaling is better suited for low-dimensional systems. As shown in Fig. 6, the Carré-Souletie analysis allowed to obtain plausible results also below the transition temperature.

For **2** the value of the critical exponent γ was found to be close to 1.0. Such a small value of γ was reported in Ref. 21, where systems involving noncollinearity of constituent spins were investigated. This places compound **2** close to the recently established universality classes N2C (XY anisotropic chiral) or N3C (Heisenberg chiral).[21] The critical exponent γ for **1** is higher than the values expected for the standard universality classes ($\gamma \sim 1.24$ for Ising, 1.32 for XY, and 1.38 for Heisenberg spins). However, it is placed consistently be-

TABLE I. Critical scaling of magnetic susceptibility as revealed by classical analysis (CL) and modified analysis put forward by CS.

Scaling	CL		CS	
Compound	T_c (K)	γ	T_c (K)	γ
1	32.6(5)	1.63(1)	33.3(2)	1.67(2)
2	39.8(1)	1.05(2)	40.0(1)	0.86(1)

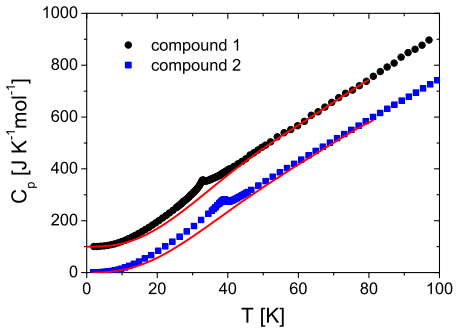

FIG. 7. (Color online) Total heat capacity at zero magnetic field for compounds **1** and **2** measured on powder samples. For clarity the heat capacity of **1** has been shifted by 100 J K^{-1} mol^{-1}. The λ-shaped anomalies signal the presence of a magnetic continuous phase transition. Solid lines are the baselines used to extract the magnetic contribution to the heat capacity (see text).

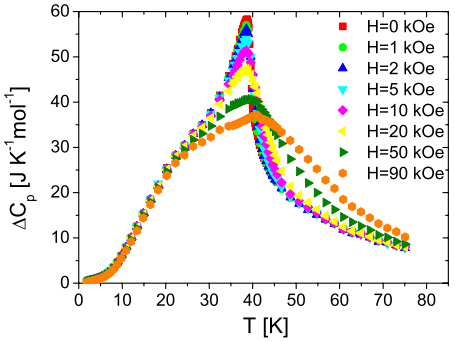

FIG. 8. (Color online) Magnetic contribution to the total heat capacity of **2** for an array of applied field values. The anomaly is suppressed and shifted toward higher temperatures with increasing applied field implying a ferromagnetic character of exchange interactions.

tween $\gamma_{\perp}(\approx 0.67)$ and $\gamma_{\parallel}(\approx 2.2)$ found in the single-crystal study for the direction perpendicular and parallel to the double layers, which were pointed out to coincide with the Monte Carlo results for systems with strong easy-plane anisotropy.[14] The transition temperatures determined from the scaling behavior (see Table I) are fully consistent with the values implied by the inflection points of the ac susceptibility curves. Figure 6 shows also the experimental data below the transition points. For both compounds the alignment of the data is clearly seen. However, there is a significant difference in their behavior. For **2** the points below and above T_c define the same line indicating the equality of the corresponding γ and γ' exponents. By contrast, for **1** clearly different slopes are observed for points below and above the transition signaling a distinct critical scaling in these regions, which may be expected for the BKT transition. The character of critical fluctuations is different below and above the BKT transition. Just below the transition there is a dense gas of bound vortex-antivortex pairs, which may be imagined to preclude spin fluctuations, hence the sudden drop of the gamma exponent. Both classical and modified scaling laws imply consistently a reduced value of γ' close to 0.2. By contrast, above the transition the pairs become unbound giving rise to less restricted fluctuations, which is signaled by the enhanced value of the gamma exponent.

V. HEAT CAPACITY

For **2** in zero applied field a well-defined λ-shaped anomaly in heat capacity was detected at 38.7 K (the peak position), see Fig. 7, proving unambiguously the presence of a magnetic continuous phase transition. The transition temperature is consistent with the value found in the magnetic measurement. To extract the magnetic excess heat capacity ΔC_p, the observed C_p values within the range 46.6–75.0 K, above the magnetic phase transition temperature, can be expressed by the sum of the lattice heat capacity—C_p (lattice), and the magnetic heat capacity due to short-range order—C_{mag} (short-range order). C_p (lattice) can be expressed by a polynomial function of temperature with cubic and higher order terms whereas C_{mag} (short-range order) can be expressed by a term proportional to T^{-2}. Thus the observed heat capacity within the range of 46.6–75.0 K can be described as

$$C_p = C_p(\text{lattice}) + C_{\mathrm{mag}}(\text{short-range order}) = \sum_{i=3}^{n} a_i T^i + bT^{-2}. \tag{4}$$

The fit of Eq. (4) with $n=6$ to the observed heat capacity yielded

$$C_p(\text{lattice})/\text{J K}^{-1}\,\text{mol}^{-1} = +1.3066\times 10^{-2}\left(\frac{T}{\text{K}}\right)^3 - 3.7262\times 10^{-4}\left(\frac{T}{\text{K}}\right)^4 + 4.0868\times 10^{-6}\left(\frac{T}{\text{K}}\right)^5 - 1.6173\times 10^{-8}\left(\frac{T}{\text{K}}\right)^6, \tag{5}$$

and $b=45.4959\times 10^3$ J K mol^{-1}. The lattice heat capacity thus determined for estimating the magnetic heat capacity is shown in Fig. 7 as the solid curve. The magnetic contribution ΔC_p was calculated by subtracting from the observed heat capacity the lattice heat capacity given by Eq. (5). Figure 8 shows the excess heat capacity for an array of applied field values. In order to calculate the experimental value of entropy change associated with the transition at zero magnetic field the following procedure has been carried out. First we fitted function $fT^{3/2}$ to the zero-field data in the range of 3.1–4.8 K. This form of function corresponds to the low-temperature contribution from spin-wave excitations $C_{SW} \propto T^{d/n}$ for a 3D ferromagnet ($d=3$, $n=2$), where d denotes the dimensionality of the spin lattice and n is the exponent in the magnonic dispersion relation. The best fit implied $f=0.1172$ J $K^{-5/2}$ mol^{-1}. This function was next used to estimate the contribution to the entropy in the temperature range 0–3.1 K. It was found to amount to 0.43 J K^{-1} mol^{-1}. The entropic contribution in the temperature range 3.1–75.0 K was obtained by numerical integration of the area under the excess heat-capacity peak $S=\int \Delta C_p d \ln T$. It amounts to 49.24 J K^{-1} mol^{-1}. Finally the high-temperature excess heat

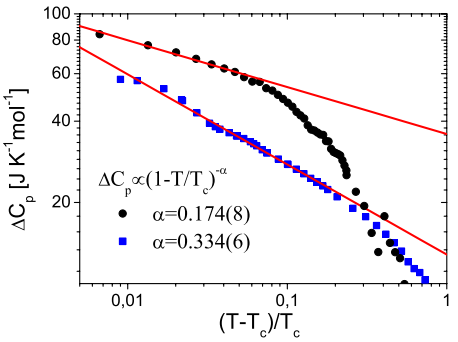

FIG. 9. (Color online) Scaling plots for the zero-field magnetic heat capacity of **1** (circles) and **2** (squares). To avoid overlap of the data the heat-capacity values of **1** were multiplied by factor 1.5. The positive values of the α exponent suggest the presence of noncollinearity in spin arrangement.

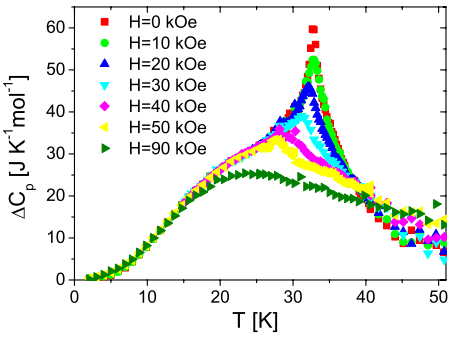

FIG. 10. (Color online) Magnetic contribution to the total heat capacity of **1** for an array of applied field values. The magnetic field is applied in the direction perpendicular to the double layers. The anomaly is suppressed and shifts toward lower temperatures with increasing applied field. This behavior is due to the presence of the strong easy-plane anisotropy.

capacity bT^{-2} was used to estimate the entropic contribution above 75 K. This last contribution is 4.04 J K^{-1} mol^{-1}. The total entropy change thus amounts to 53.71 J K^{-1} mol^{-1}. The expected value of entropy change corresponds to that for nine one-half spins [seven originating from Cu(II) ions and two from W(V) ions] yielding $S=R\ln(2J+1)^9$ equal to 51.87 J/K mol for $J=1/2$. The observed entropy change compares well with the value predicted theoretically. Let us note that the λ-type anomaly is shifted toward higher temperatures by the application of magnetic field, which points to the ferromagnetic character of exchange interactions. The scaling analysis of the magnetic excess capacity for zero applied field yielded a large positive value of $\alpha=0.332$, see Fig. 9. This again is in agreement with sizable positive values of that exponent found in Monte Carlo simulations for stacked triangular antiferromagnet, where noncollinearity of the spins is present.[21] In the case of **1** both ferromagnetic and antiferromagnetic interactions were involved. The former were responsible for the ordering within the double layers whereas the latter determining the interbilayer interactions accounted for the observed metamagnetic behavior.[14,22] To extract the magnetic contribution to the heat capacity an analogous procedure as for **2** was applied. The fit of Eq. (5) with $n=6$ to the heat capacity measured on powder sample (see Fig. 7) in the temperature range 45–82 K yielded

$$C_p(\text{lattice})/\text{J K}^{-1}\ \text{mol}^{-1} = +1.6362\times10^{-2}\left(\frac{T}{\text{K}}\right)^3 - 4.8149\times10^{-4}\left(\frac{T}{\text{K}}\right)^4 + 5.3554\times10^{-6}\left(\frac{T}{\text{K}}\right)^5 - 2.1211\times10^{-8}\left(\frac{T}{\text{K}}\right)^6, \quad (6)$$

and $b=12.7443\times10^3$ J K mol^{-1}. The lattice heat capacity determined in this way is shown in Fig. 7 as the solid curve. The magnetic contribution ΔC_p was calculated by subtracting from the heat capacity measured on a single crystal with the external field perpendicular to the double layers the lattice heat capacity given by Eq. (6). Figure 10 shows the excess heat capacity for an array of applied field values. The magnetic heat-capacity peaks are shifted toward lower temperatures while applying the magnetic field in the direction perpendicular to the double layers, see Fig. 10. This is attributed to the presence of the strong easy-plane anisotropy with the applied field reducing the spontaneous in-plane alignment of magnetic moments. We proceeded along the same lines as for **2** to calculate the excess entropy associated with the zero-field anomaly. It was found to amount to 43.49 J K^{-1} mol^{-1} and compares well with the value of 46.10 J K^{-1} mol^{-1} expected for eight spins one-half per formula unit. The critical scaling analysis of the zero-field heat capacity reveals, similarly to **2**, a positive value of the α exponent equal to 0.174(8), see Fig. 9.

In conclusion, the additional Cu(II) ions located between the bilayers give rise to the reinforcement of exchange interaction evidenced by the positive shift of the transition temperature. Besides, the character of interaction between the double layers is changed from antiferromagnetic to ferromagnetic.

VI. MUON SPIN-ROTATION SPECTROSCOPY

Muon spin precession measured under zero external field gives valuable information about order parameters, local internal fields, magnetic fluctuations in the neighborhood of a phase transition and spin dynamics.[23–25] This method revealed unique critical fluctuations in molecular magnets impossible to see by other methods. Fully spin-polarized muons are subject to precession in a local field at a muon stopping site. The trajectory of the precession is traced by the positron emission and registered by the backward and forward detectors. The time evolution of the spin polarization of the implanted muons was detected by measuring the asymmetry function $A(t)$ given by

$$A(t)=\frac{N_B-N_F}{N_B+N_F}, \quad (7)$$

where N_F and N_B denote the numbers of decay positrons emitted forward and backward, respectively. Figure 11 shows the muon spin relaxation detected in the vicinity of the mag-

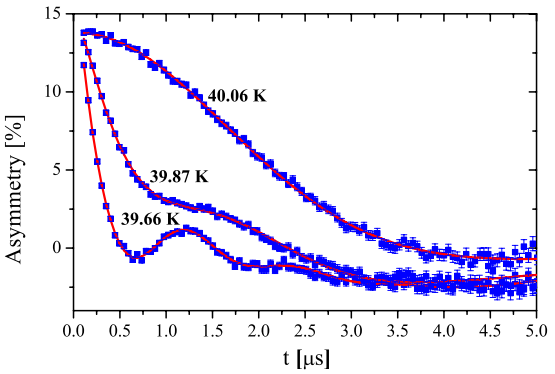

FIG. 11. (Color online) Time dependence of the muon asymmetry function observed in the vicinity of the transition point of **2** under zero field. The onset of spontaneous oscillations in the relaxation signal marks the transition to an ordered phase. Solid lines show the fits to the relaxation function given by Eq. (8) where a single precession frequency was assumed.

netic transition. Spontaneous oscillations observed in the time dependence of the asymmetry function $A(t)$ below 39.87 K indicate the presence of local fields static on the microsecond scale, marking the transition to the ordered phase. It was checked that these oscillations require a single precession frequency ω

$$A(t) = A_0 + A_1 \cos(\omega t + \phi)e^{-\lambda t}, \tag{8}$$

where $\omega = \gamma_\mu B$, $\gamma_\mu = 2\pi \times 1.355 \times 10^8$ (T s^{-1}) is the muon gyromagnetic ratio, B denotes the magnitude of the local field, and λ is the relaxation rate. The presence of one dominant frequency suggests a single site of muon implantation. It is in contrast to compound **1** where two frequencies were observed, which may be understood in terms of a single stopping site embedded in two distinct local domains with magnetic moments pointing in the a or c crystallographic directions.[15] Temperature dependence of the corresponding local magnetic fields are depicted in Fig. 12. In order to describe the critical behavior it was fitted to the function

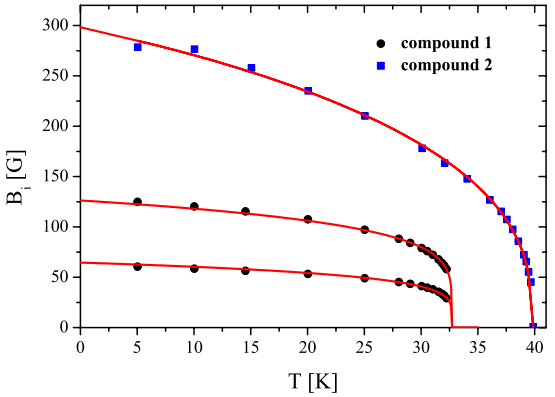

FIG. 12. (Color online) Temperature dependence of the local magnetic fields as inferred from the μSR experiment for **1** and **2**. Solid lines show the fits to the phenomenological law given in Eq. (9). For **1** two local fields were detected whereas for **2** only one local field was observed.

$$B(T) = B(0)\left[1 - \left(\frac{T}{T_c}\right)^{\sigma}\right]^{\beta}. \tag{9}$$

Parameter σ relates to the low-temperature properties governed by spin-wave excitations while parameter β determines the asymptotic behavior near the transition. The best-fit parameter values found for **2** are: $\sigma = 1.10(9)$, $\beta = 0.373(8)$, $T_c = 39.86(1)$ K, and $B(0) = 294(2)$ G. The value of β critical exponent is close to that known for the universality class of the isotropic Heisenberg model in 3D. The parameter values determined for **1** (Ref. 15) are: $\beta = 0.237(12)$, $\alpha = 1.84(15)$, $B_1(0) = 121.0(6)$ G, and $B_2(0) = 61.7(7)$ G. The value of exponent β implies that the compound can be classified to the group of 2D systems with XY exchange anisotropy, thus providing a possibility for the unique Berezinskii-Kosterlitz-Thouless transition.

VII. COMBINED SCALING OF EXCESS ENTROPY AND ORDER PARAMETER

The main benefit from the μSR spectroscopy performed in zero field is the direct insight into the thermal behavior of the order parameter related to the nonvanishing internal fields marking unambiguously the onset of the transition to the ordered phase. This crucial information can be combined with that concerning the entropy of the system inferred from the complementary calorimetric measurements to yield further characteristics of the critical behavior. On the basis of the critical laws for specific heat and order parameter it was demonstrated in Ref. 26 that the ratio of excess entropy and the square of order parameter is expected to obey a specific scaling law below the transition point T_c

$$\frac{\Delta S}{Q^2} \propto \left(1 - \frac{T}{T_c}\right)^{\kappa}. \tag{10}$$

where κ is the corresponding critical exponent related to critical exponents α and β

$$\kappa = \begin{cases} 1 - \alpha - 2\beta & \alpha > 0 \\ 1 - 2\beta & \alpha \leq 0. \end{cases} \tag{11}$$

Equivalently, the scaling relation between both quantities can be expressed by the following law:

$$\Delta S \propto Q^{2\kappa'}, \tag{12}$$

where

$$\kappa' = \begin{cases} (1 - \alpha)/2\beta & \alpha > 0 \\ 1/2\beta & \alpha \leq 0. \end{cases} \tag{13}$$

The excess entropy was calculated numerically from the heat-capacity data

$$\Delta S = \int_T^{T_c} \frac{\Delta C_p}{T'} dT' = \int_0^{\epsilon} \frac{\Delta C_p}{1 - \epsilon'} d\epsilon', \tag{14}$$

where $\epsilon = 1 - T/T_c$. As the multiplicative factors are irrelevant in the scaling analysis, the thermal dependence of the order parameter was replaced by that of the local field obtained from the μSR experiment, see Fig. 12. Figures 13 and 14

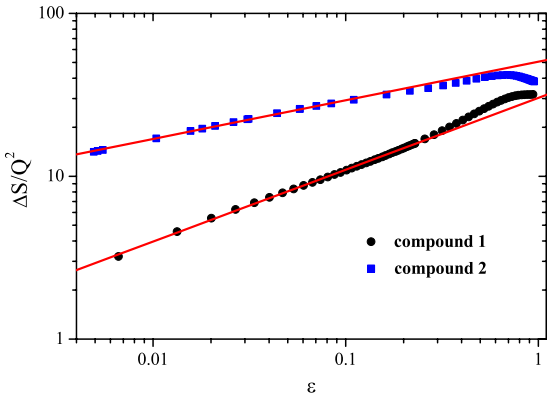

FIG. 13. (Color online) $\Delta S/Q^2$ vs $\frac{T_c-T}{T_c}$ in log-log plot for **1** and **2**. For both compounds the experimental points tend to align while approaching the transition temperature, which signals the algebraic scaling behavior. Solid lines show the corresponding linear fits.

show that the experimental points tend to align while approaching the transition temperature for both compounds. The ensuing asymptotic linear behavior for **2** yields the following values of the exponents: $\kappa=0.241(5)$ and $\kappa'=1.295(3)$. The value of exponent κ alone fails to pinpoint the corresponding universality class as for both Ising-3D and Heisenberg-3D models the same value of 0.26 is expected.[26] It is the value of exponent κ', which is close to that predicted for Heisenberg-3D model ($\approx$1.31), that suggests the Heisenberg-3D universality class. This, in turn, would point out to the negative value of the α exponent, however, its value found independently from the calorimetric measurement is positive and quite large. Using Eqs. (11) and (13) and the values of $\alpha=0.33$ and $\beta=0.373$ one obtains $\kappa=-0.08$ and $\kappa'=0.9$ which are both lower than those found from the scaling analysis. On the other hand, using the Rushbrook relation ($\alpha+2\beta=2-\gamma$), and expressing the rhs of Eqs. (11) and (13) in terms of exponents $\gamma=1.05$ and $\beta=0.373$ leads to $\kappa=0.05$ and $\kappa'=1.08$. In conclusion, the value of κ' calculated on the basis of α, β, and γ is in reasonable agreement with that found directly from the scaling plot whereas for κ an apparent discrepancy is observed.

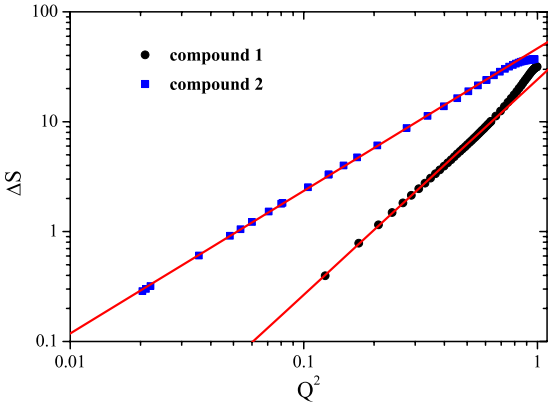

FIG. 14. (Color online) The log-log plot of the excess entropy as function of the square of order parameter for **1** and **2**. For both compounds the alignment of the data points while approaching the transition temperature is clearly visible. Solid lines show the corresponding linear fits.

The same scaling analysis was repeated for **1**. Figures 13 and 14 show the corresponding log-log plots. The experimental points tend to align while approaching the transition temperature, which is not obvious for two reasons. Firstly, it was established[14] that this compound is most closely related to the XY-2D universality class with a possible topological transition of the Berezinskii-Kosterlitz-Thouless type. Secondly, the discussed scaling behavior involves the critical region below the transition point, and no such scaling was theoretically derived for the BKT transition. The solid lines in Figs. 13 and 14 show the corresponding linear fits, from which the values of critical exponents are inferred: $\kappa=0.443(2)$ and $\kappa'=1.965(5)$. The values of κ and κ' are substantially higher than those expected for the standard universality classes with the XY-3D model being the closest one to this case.[26] However, as mentioned above, this compound is a unique system revealing the signatures of the BKT transition,[14,15] and the critical exponents for the combined scaling of excess entropy and order parameter have been experimentally determined for such a system. The values of κ and κ' calculated from Eqs. (11) and (13) using the values of α and β found from the corresponding scaling relations are 0.35(3) and 1.7(1), respectively. They agree well with the values determined from the combined scaling of excess entropy and order parameter.

VIII. CONCLUSION

We presented the results obtained by complementary experimental methods for two structurally related compounds based on octacyanotungstate and copper ions. They were employed to get insight into the critical behavior. Firstly, let us note that the exponents $\alpha=0.334$, $\beta=0.373$, and $\gamma=1.05$ found from the corresponding scaling laws for compound **2** satisfactorily reproduce the Rushbrook scaling relation, yielding $\alpha+2\beta+\gamma=2.13(4)$, which falls close to the expected value of 2. An interesting finding is the fact that although compound **2** may contain diamagnetic centers and the copper sites located between the double layers are only partially occupied it still reveals critical features close to the universality class of 3D Heisenberg model. That is consistently demonstrated by both the critical scaling of order parameter ($\beta=0.373$) and the combined scaling of excess entropy and order parameter ($\kappa'=1.295$). This evidence is of relevance to the general theory of critical phenomena, as it shows that even imperfect magnetic network yet satisfying the requirement of full 3D connectivity is sufficient to remain in the class of 3D models. The same features of the magnetic network, resulting possibly in its disorder, seem to account for the suppressed intensity of magnetic peaks, which prevents their identification in the diffraction pattern. On the other hand, the unusually small γ exponent found from the ac susceptibility signal points presumably out to the presence of noncollinearity in the spin arrangement. This is suggested by the comparison of the critical exponents to those calculated in the Monte Carlo simulations for the stacked triangular antiferromagnet (STA), where noncollinearity originates from the inherent spin frustration,[21] see Table II. The proximity to these recently established uni-

TABLE II. Critical exponents for **1** and **2** (determined in this work) and for two STA model systems [calculated (Ref. 21)]. N2C and N3C stand for the universality classes corresponding to the chiral model with XY exchange anisotropy and the chiral model with isotropic Heisenberg exchange interaction, respectively. The values of exponents κ and κ' were calculated for the first two entries using the relations $\kappa=\gamma-1$ and $\kappa'=1+\frac{\gamma-1}{2\beta}$.

	α	β	γ	κ	κ'
3D N2C	0.34(6)	0.253(1)	1.13(5)	0.13(5)	1.26(10)
3D N3C	0.24(8)	0.30(2)	1.17(7)	0.17(7)	1.28(13)
Compound **2**	0.334(6)	0.373(8)	1.05(2)	0.241(5)	1.295(3)
Compound **1**	0.174(8)	0.237(12)	1.63(1)	0.439(2)	1.956(5)

versality classes is further evidenced by the comparable values of the κ and κ' exponents.

Another important finding is the experimental verification of the combined scaling of excess entropy and order parameter for compound **1**. As it exhibits the unique Berezinskii-Kosterlitz-Thouless transition,[14,15] the corresponding critical exponents κ and κ' are reported. Their values are consistent with those of β and α determined from the independent scaling relations. The check of the Rushbrook identity yields for this compound $\alpha+2\beta+\gamma=2.28(4)$. The deviation from the expected value is larger than that obtained for **2**. However, it may be attributed to the fact that the scaling law for susceptibility in the BKT transition has an exponential form instead of an algebraic form.

ACKNOWLEDGMENTS

This work has been partially supported by the Polish Ministry of Science and Higher Education within Research Projects No. 0087/B/H03/2008/34 and No. 1535/B/H03/2009/36.

*mariusz.czapla@ifj.edu.pl

[1] S. Ferlay, T. Mallah, R. Quahes, P. Veillet, and M. Verdaguer, Nature (London) **378**, 701 (1995).
[2] R. Sessoli, D. Gatteschi, A. Caneschi, and M. A. Novak, Nature (London) **365**, 141 (1993).
[3] C. Coulon, H. Miyasaka, and R. Clérac, Struct. Bonding (Berlin) **122**, 163 (2006).
[4] L. Bogani, A. Vindigni, R. Sessoli, and D. Gatteschi, J. Mater. Chem. **18**, 4750 (2008).
[5] O. Sato, T. Iyoda, A. Fujishima, and K. Hashimoto, Science **272**, 704 (1996).
[6] K. Hashimoto and H. Ohkoshi, Philos. Trans. R. Soc. London, Ser. A **357**, 2977 (1999).
[7] T. Hozumi, K. Hashimoto, and S. Ohkoshi, J. Am. Chem. Soc. **127**, 3864 (2005).
[8] B. Sieklucka *et al.*, Cryst. Eng. Comm. **11**, 2032 (2009).
[9] D. Pinkowicz, R. Podgajny, M. Bałanda, M. Makarewicz, B. Gaweł, W. Łasocha, and B. Sieklucka, Inorg. Chem. **47**, 9745 (2008).
[10] T. Kashiwagi, S. Ohkoshi, H. Seino, Y. Mizobe, and K. Hashimoto, J. Am. Chem. Soc. **126**, 5024 (2004).
[11] S.-L. Ma, S. Ren, D.-Z. Liao, and S.-P. Yan, Struct. Chem. **20**, 145 (2009).
[12] B. Sieklucka, R. Podgajny, P. Przychodzeń, and T. Korzeniak, Coord. Chem. Rev. **249**, 2203 (2005).
[13] P. Przychodzeń, T. Korzeniak, R. Podgajny, and B. Sieklucka, Coord. Chem. Rev. **250**, 2234 (2006).
[14] M. Bałanda, R. Pełka, T. Wasiutyński, M. Rams, Y. Nakazawa, Y. Miyazaki, M. Sorai, R. Podgajny, T. Korzeniak, and B. Sieklucka, Phys. Rev. B **78**, 174409 (2008).
[15] F. L. Pratt, P. M. Zieliński, M. Bałanda, R. Podgajny, T. Wasiutyński, and B. Sieklucka, J. Phys.: Condens. Matter **19**, 456208 (2007).
[16] R. Podgajny, T. Korzeniak, M. Bałanda, T. Wasiutyński, W. Errington, T. J. Kemp, N. W. Alcock, and B. Sieklucka, Chem. Commun. (Cambridge) **2002**, 1138.
[17] R. Podgajny *et al.*, J. Mater. Chem. **17**, 3308 (2007).
[18] F. L. Pratt, Physica B **289-290**, 710 (2000).
[19] E. Carre and J. Souletie, J. Magn. Magn. Mater. **72**, 29 (1988).
[20] M. Drillon, P. Panissod, P. Rabu, J. Souletie, V. Ksenofontov, and P. Gutlich, Phys. Rev. B **65**, 104404 (2002).
[21] H. Kawamura, J. Phys. Soc. Jpn. **61**, 1299 (1992).
[22] R. Pełka, M. Bałanda, T. Wasiutyński, Y. Nakazawa, M. Sorai, R. Podgajny, and B. Sieklucka, Czech. J. Phys. **54**, D595 (2004).
[23] F. L. Pratt, P. J. Baker, S. J. Blundell, T. Lancaster, M. A. Green, and M. Kurmoo, Phys. Rev. Lett. **99**, 017202 (2007).
[24] T. Lancaster, S. J. Blundell, P. J. Baker, D. Prabhakaran, W. Hayes, and F. L. Pratt, Phys. Rev. B **75**, 064427 (2007).
[25] F. L. Pratt, T. Lancaster, P. Baker, S. Blundell, W. Kaneko, M. Ohba, S. Kitagawa, S. Ohira-Kawamura, and S. Takagi, Physica B **404**, 585 (2009).
[26] J. M. Martín-Olalla, F. J. Romero, S. Ramos, M. C. Gallardo, J. M. Perez-Mato, and E. K. H. Salje, J. Phys.: Condens. Matter **15**, 2423 (2003).